ACS Photonics

pubs.acs.org/journal/apchd5

Article

Engineering the Luminescence and Generation of Individual Defect Emitters in Atomically Thin MoS_2

Julian Klein,*,○ Lukas Sigl,○ Samuel Gyger, Katja Barthelmi, Matthias Florian, Sergio Rey, Takashi Taniguchi, Kenji Watanabe, Frank Jahnke, Christoph Kastl, Val Zwiller, Klaus D. Jöns, Kai Müller, Ursula Wurstbauer, Jonathan J. Finley, and Alexander W. Holleitner*

Cite This: *ACS Photonics* 2021, 8, 669–677

Read Online

ACCESS | Metrics & More | Article Recommendations | Supporting Information

ABSTRACT: We demonstrate the on-demand creation and positioning of photon emitters in atomically thin MoS_2 with very narrow ensemble broadening and negligible background luminescence. Focused helium-ion beam irradiation creates 100s to 1000s of such mono-typical emitters at specific positions in the MoS_2 monolayers. Individually measured photon emitters show antibunching behavior with a $g^2(0) \sim 0.23$ and 0.27. From a statistical analysis, we extract the creation yield of the He-ion induced photon emitters in MoS_2 as a function of the exposed area, as well as the total yield of single emitters as a function of the number of He ions when single spots are irradiated by He ions. We reach probabilities as high as 18% for the generation of individual and spectrally clean photon emitters per irradiated single site. Our results firmly establish 2D materials as a platform for photon emitters with unprecedented control of position as well as photophysical properties owing to the all-interfacial nature.

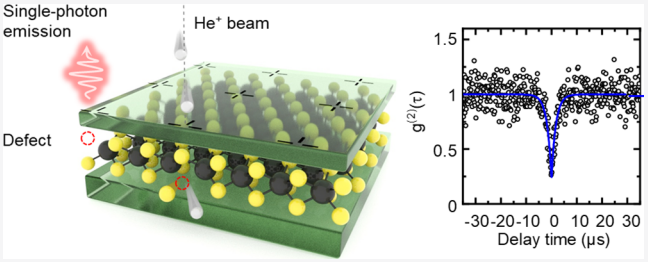

KEYWORDS: *2D materials, molybdenum disulfide, quantum emitter, He-ion irradiation, defect generation, vdW heterostructure*

Real-world quantum applications, e.g., on-chip quantum networks and quantum cryptography, necessitate large scale integrated single-photon sources with a nanoscale footprint for modern information technology.[1−3] While on-demand and high fidelity generation of atomic scale single-photon sources in conventional 3D materials suffer from uncertainties in the depth positioning due to the crystals' dimensionality,[4−6] layered 2D materials can host point-like centers with inherent confinement to a sub-nm plane.[7−11] Developing scalable approaches for the generation of single-photon emitters in solid-state materials is a longstanding goal in the field of quantum nanophotonics.[4−6,12−16] Such emitters attract significant attention due to their prospective use in miniaturized quantum photonic systems. A prominent example is diamond, with the most actively studied color centers being the NV and SiV.[2,3] Such color centers are typically induced by ion implantation and subsequent annealing with the emitters being buried in a bulk matrix several tens of nanometers below the surface.[4,6] Therefore, their creation is often probabilistic and accompanied by significant lateral and axial positioning inaccuracies from ion straggling effects and annealing for vacancy center formation. Ultimately, such inaccuracies render their efficient interfacing to nanophotonic circuits challenging and may also deteriorate the emitters' electronic and optical properties, which are impacted by their distance from the surface.[5,6]

A natural workaround is to reduce the physical dimensionality of the material. In this context, 2D materials are ideal candidates for hosting single-photon emitters that are inherently restricted to a sub-nm thin material.[17] In recent years, luminescence from spatially localized emitters in hBN,[18] WSe_2,[7−11] and GaSe[19] has been observed. While deterministic placement of the emission centers has been shown in WSe_2, WS_2, and hBN by creating local exciton confinement potentials,[12−14,20] their 2D character is partially lost because of the necessary strain profile and the precise origin of emission remains subject to debate. Similarly, localized, yet randomly occurring, single-photon emission has been observed near wrinkles and edges of hBN and GaSe.[15,19] In layered hBN, various attempts to deterministically localize the emitters have been challenging so far owing to the rigidity of the material.[15,21] Moreover, emitters in exfoliated and solution prepared hBN exhibit strong inhomogeneous ensemble broadening and the spatial occurrence of emitters remains

Received: December 15, 2020
Published: January 21, 2021

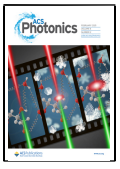

https://dx.doi.org/10.1021/acsphotonics.0c01907
ACS Photonics 2021, 8, 669–677

largely random,[16,18,21] most likely reflecting a diverse typology of different defects.[15,18]

Here, we demonstrate a highly local creation of photon emitters in atomically thin MoS_2 using a focused He-ion beam. The emitters show narrow optical signatures and significantly reduced ensemble broadening. For generating defects, we utilize a helium-ion microscope (HIM) which provides a nanometer-focused stream of He ions that penetrates through the encapsulation layer without noteworthy loss of its beam properties (see Supporting Information S1).[22,23]

We investigate two types of samples: (A) hBN/MoS_2/hBN that is irradiated after hBN encapsulation (Figure 1a) and (B)

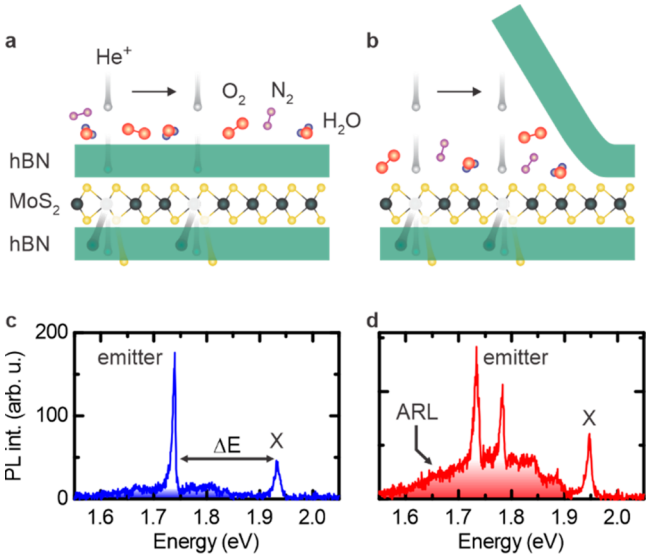

Figure 1. Atomically thin MoS_2 as a platform for positioned photon emitters with a negligible background. (a) Schematic He-ion irradiation and vacancy defect creation. Impact of layer sequence of the investigated van der Waals heterostructures and focused He-ion induced generation of photon emitters. He-ion irradiation after hBN encapsulation (type A) results in clean interfaces with significantly reduced contamination from adsorbates. (b) He-ion irradiation prior to encapsulation (type B) promotes the interaction of defects with ambient contaminants. (c) Typical low temperature (15 K) PL spectrum of irradiated hBN/MoS_2/hBN after encapsulation. The spectrum features neutral exciton emission (X) and the photon emission of single sites. Adsorbate-related luminescence (ARL) is suppressed owing to the hBN encapsulation. (d) The PL spectrum from a heterostructure exposed prior to encapsulation reveals inhomogeneous emission with multiple emission lines distributed over a broader spectral window and significant ARL.

MoS_2 on hBN that is first irradiated prior to full encapsulation with hBN (Figure 1b). The encapsulation procedure reduces the background emission from adsorbate-related luminescence (ARL) (Figure 1c,d),[24,25] the so-called L-band emission. Typically, after the irradiation of a non-encapsulated monolayer MoS_2, accumulation of adsorbates on the defective surface like N_2, O_2, and H_2O is expected,[22] which can manifest in chemically altered defect state morphology or simply through ambient passivation of sulfur vacancies with oxygen.[26,27] As recently demonstrated combining scanning tunneling microscopy and He-ion irradiation,[28] the irradiation of MoS_2 with helium ions creates both sulfur and molybdenum vacancies in the MoS_2 with sub-10 nm resolution. Importantly, while sulfur vacancies seemed to be the most abundant defect in TMDCs, they tend to be all passivated by oxygen atoms.[26] Hence, sulfur vacancies as generated by He-ion irradiation are well preserved when additionally encapsulated in hBN. The current understanding is that the defect emission in MoS_2 is very likely originating from nonpassivated sulfur vacancies. Figure 1c demonstrates that, for local generation through the readily assembled hBN/MoS_2/hBN heterostructure, the luminescence features the emission from excitons (X) and a single defect related very narrow emission line with negligible background emission. Importantly, we show below that such individually measured photon emitters show single-photon statistics with $g^{(2)} < 0.5$ and can be therefore regarded as single-photon emitters. The high optical quality of our emitters is most likely a consequence of the reduction of contaminants from the van der Waals interfaces that are squeezed out during the stacking process, resulting in electronically homogeneous heterointerfaces.[24]

We investigate the emission statistics of emitters obtained from spatially resolved μ-PL mappings of nominally identical samples for irradiation prior to and after hBN encapsulation. For both sample configurations, we irradiate circular areas with diameters ranging from 700 nm down to 100 nm with a pitch of 2 μm and a constant He-ion dose of $\sigma = 5 \times 10^{12}$ ions cm^{-2}, which is far below the threshold for modifying the free exciton emission.[22] By reducing the irradiated area, we demonstrate emission from few emission lines down to well-defined ("spectrally clean") individual emitters within the resolution of our laser spot ($d_{laser} \sim 700$ nm). Figure 2a shows spatially resolved μ-PL mappings of a hBN/MoS_2/hBN of type (A) for exposure diameters of 700, 400, and 200 nm. The PL is spectrally integrated between 1.7 and 1.88 eV to reveal emission from He-ion induced emitters (Supporting Information, Figure S2). The He-ion irradiation manifests in spatially activated emitters clearly following the writing pattern from the HIM. Note that the emitters do not stem from He-ion irradiated hBN (Supporting Information, Figure S3) and that slight deviations in the occurrence of the localized emission only originate from sample drift in confocal PL mapping.

Typical spectra of fields with a 700 nm diameter reveal multiple overlapping emission lines that are within the point spread function of our laser spot. However, for the smaller diameters $\leq$ 200 nm, we observe distinct individual emission lines at ~1.75 eV corresponding to a statistical energy detuning of $\Delta E = E(\mathrm{X}) - E(\mathrm{Emitter}) = 194 \pm 1$ meV. Importantly, we consistently find the ARL to be reduced for He-ion irradiation through the fully assembled heterostructures. For comparison, Figure 2c shows a μ-PL mapping of a nominally identical sample but of type B. Here, the quality of the spectra is limited by the spectrally broad ARL, and the photon emitters are distributed more widely in emission energy as evident from the emission statistics obtained from peak finder algorithms. Statistics obtained from the sample irradiated after encapsulation (type A in Figure 2e) reveal a narrow inhomogeneous ensemble distribution I of the emitters at an energy detuning $\Delta E = 194 \pm 1$ meV and with an fwhm of 31 ± 1 meV. The corresponding very similar distribution of absolute energies is shown in Supporting Information Figure S4. This is in strong contrast to samples of type B (Figure 2f). Here, the emission distribution at the main energy detuning is significantly broadened with an fwhm of 38 ± 3 meV, and the second, similarly intense emission distribution II at $\Delta E = 139 \pm 2$ meV emerges with an fwhm of 46 ± 3 meV. The emission distribution II is almost entirely absent in the irradiated sample after encapsulation (Figure 2e), and we attribute it to stem

https://dx.doi.org/10.1021/acsphotonics.0c01907
ACS Photonics 2021, 8, 669−677

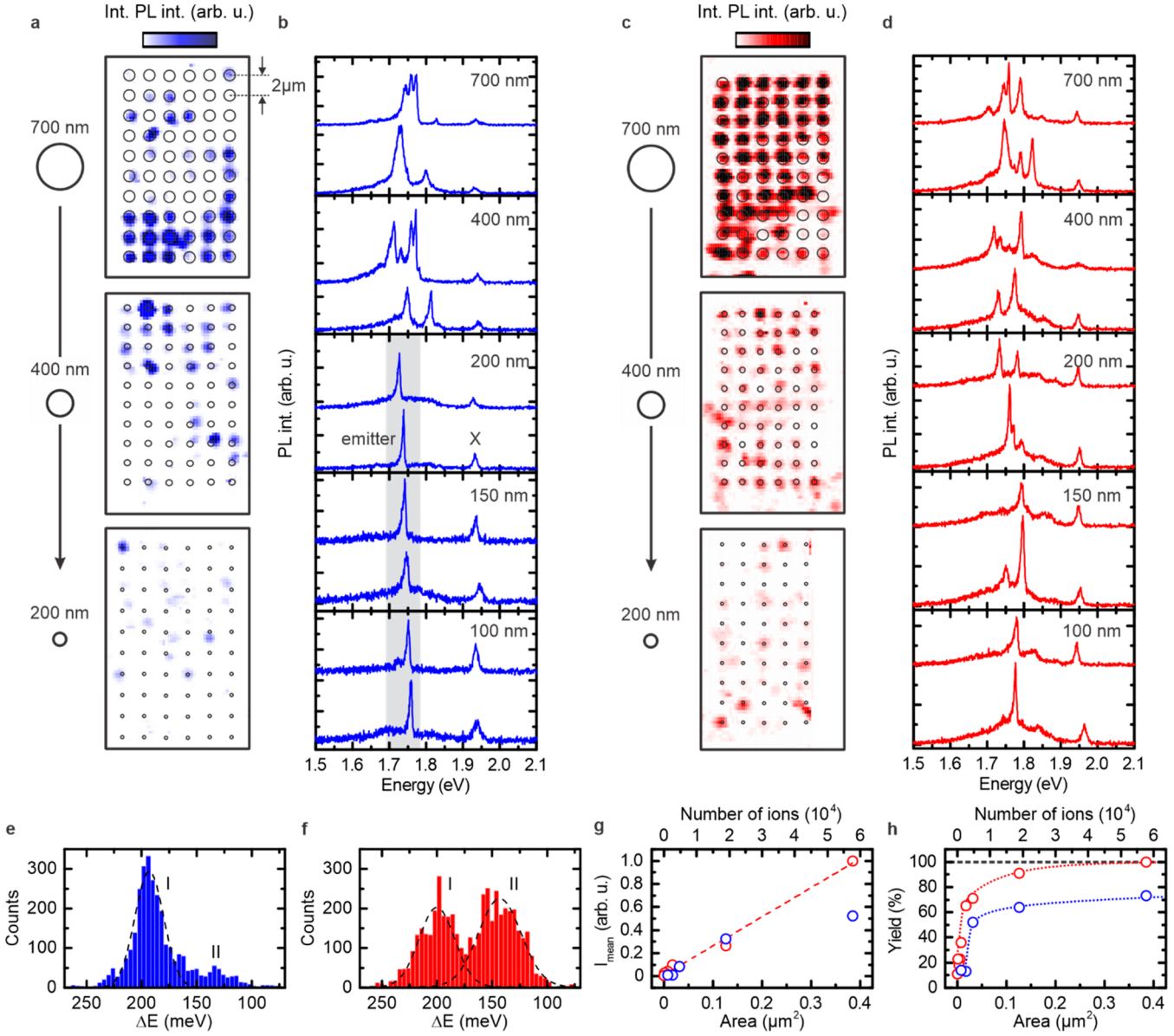

Figure 2. Ensemble generation of photon emitters with high yield and narrow inhomogeneous ensemble broadening. (a) Spatially resolved low temperature (15 K) μ-PL spectroscopy of emitters in locally He-ion irradiated hBN/MoS_2/hBN (type A). The ion dose is kept constant at $\sigma = 5 \times 10^{12}$ ions cm^{-2}, and the exposed area is varied. Circular exposures with varying diameters are arranged in a matrix with a pitch of 2 μm. Slight deviations from the He-ion induced pattern observed in the PL mappings are from drift during the measurement. (b) Typical PL spectra for circular areas of varying diameters are shown (700, 400, 200, 150, and 100 nm). Spectra from the largest areas exposed contain multiple emitters, whereas fields with $d \leq 200$ nm are in the limit of individual photon emitters with reproducible spectral emission energies (~1.75 eV) and suppressed ARL. (c) μ-PL mapping of emitters in locally He-ion irradiated MoS_2 prior to encapsulation (type B). The same dose and diameters were used. (d) Typical PL spectra for circular areas of varying diameters are shown. Spectra exhibit multiple emitters that are widely distributed in energy with significant ARL. (e, f) Inhomogeneous ensemble broadening (energy detuning of individual emitters $\Delta E = E(\mathrm{X}) - E(\mathrm{Emitter})$) of emission. Irradiated MoS_2 after encapsulation exhibits a narrow inhomogeneous ensemble broadening distribution I with fwhm = 31 ± 1 meV centered at a detuning of $\Delta E = 194 \pm 1$ meV. Irradiation prior to full encapsulation reveals a larger ensemble broadening distribution I (fwhm = 38 ± 3 meV) with an additional spectrally broad distribution II (fwhm = 46 ± 3 meV) centered at $\Delta E = 139 \pm 2$ meV. (g) Mean integrated emitters intensity per activated field. The data suggest a linear relation of intensity and area of irradiated MoS_2 prior to encapsulation. The deviation of the last data point for the irradiated fully encapsulated MoS_2 is attributed to sample inhomogeneities. (h) Creation yield of He-ion irradiated fields as a function of area. Unity yield is highlighted with the dashed horizontal line. The colored lines are a guide to the eye.

from randomized interactions of the emitters with molecular species during the ambient exposure subsequent to He-ion irradiation and prior to full encapsulation with hBN (Figure 1b).[25] The finite value of the photon emitter distribution comes from sample inhomogeneities, like surface contamination, strain, or dielectric variations, which are natural to devices fabricated by viscoelastic stamping. Reduction of surface contamination in sample type A already results in a narrowing of the emitter distribution, reflecting a more homogeneous sample quality.

We continue to determine the probability and yield to activate emission lines in the He-ion irradiated circular areas. We expect the number of emission centers and their corresponding intensity in first approximation to scale linearly

https://dx.doi.org/10.1021/acsphotonics.0c01907
ACS Photonics 2021, 8, 669−677

with the number of ions, and hence also with the irradiated area at a constant area dose. Indeed, the mean integrated intensity of the emission lines exhibits a linear dependence on the corresponding irradiated area, or equivalently absolute number of ions for small exposure areas (Figure 2g). Moreover, statistically evaluating the percentage of activated fields (Figure 2h), we find unity creation efficiency for 700 nm for MoS_2 irradiated prior to encapsulation, and the activation efficiency for MoS_2 irradiated after encapsulation reaches values > 70%. This discrepancy is very likely due to a substantial number of emitters at an energy detuning of ΔE = 139 meV (Figure 2f) that are absent in irradiated MoS_2 after encapsulation. The origin of such emission is likely from modified "bright" defects at the detuning ΔE = 194 meV, where a complex wave function admixture for unintentional doping with functional groups shifts the emission energy. The latter possibility suggests interesting prospects for intentional manipulation of individual emitters in 2D materials by their interaction with external species. The individual emission lines created in the fully encapsulated MoS_2 show superb optical properties with narrow zero phonon lines (Figure 3a) at 10 K and a weak satellite peak at a Raman shift of ~248 cm^{-1} (energy detuning of ~31 meV).

Intriguingly, the latter line does not match with optical phonon energies,[29] but it may likely be explained by a local phonon mode (LPM) of the defect similar to hBN.[30] At lower bath temperatures (Figure 3b), the zero phonon line narrows significantly to 248 μeV at T = 1 K. The asymmetric line shape is well described with an independent boson model fit which accounts for interaction with acoustic phonons[23] (inset of Figure 3b), resulting in a Debye–Waller factor of 0.27. The excellent agreement with this model further suggests that the ion-generated emission lines in MoS_2 can be well understood with atomic physics, similar to color centers in diamond.

Moreover, the fit suggests a homogeneous (inhomogeneous) contribution of 100 μeV (188 μeV) to the line width. This is still larger than the transform limit, which can be explained by the nonresonant excitation; as for solid-state single-photon emitters, transform-limited line width is typically only observed under resonant excitation.

To unambiguously prove the nonclassical nature of light emission from our He-ion created defects, we perform a Hanburry Brown and Twiss (HBT) experiment. Figure 3c,d depicts the second-order intensity autocorrelation function $g^{(2)}(\tau)$ of a created defect under CW excitation measured at 5 K for an emission stemming from distribution I and II from Figure 2e,f. We clearly observe antibunching with a $g^{(2)}(0)$ = 0.23 ± 0.04 ($g^{(2)}(0)$ = 0.27 ± 0.10) at zero time delay (τ = 0) for the emitter from distribution I (II). Moreover, the fit suggests a long radiative recombination time of τ = 1.73 ± 0.15 μs (τ = 0.23 ± 0.05 μs) for I (II), which contrasts strongly with the ns lifetimes typically observed for other localized individual emitters in all other 2D materials[7−11,18,19] (cf. Table 1) but is similar to cold atoms and trapped ions. The observed antibunching corroborates our assumption that the narrow, ion-induced emission lines act as single-photon emitters. To estimate the lateral and axial precision with which we generate the emitters in the MoS_2 monolayer, we perform Monte Carlo simulations of beam trajectories through a thick slab of hBN to obtain the beam resolution of the primary beam (Supporting Information, Figure S1). For typical hBN thicknesses used throughout this paper (<20 nm), we obtain a primary He-ion beam resolution of <5 nm at the monolayer. Recent numerical calculations proposed that the lateral resolution to create defects in a substrate-supported monolayer MoS_2 for the beam energies (30 keV) used in our samples is <10 nm[31] which has been recently verified by scanning tunneling microscopy confirming a lateral He-ion vacancy defect creation accuracy of 9 nm.[28]

Overall, we anticipate that secondary ion processes will be the limiting factor in MoS_2 layers supported on thick substrates. We create the emitters in a readily assembled van der Waals heterostructure using spot exposures, where the exposed area only corresponds to the area of the ion beam (Figure 4). To obtain reliable statistics, we wrote arrays of 4 × 10 exposures with a pitch of 2 μm (as highlighted for field number six from the top in Figure 4a). Figure 4a shows a spectrally integrated PL map of such an irradiated sample. The number of ions per spot is varied from 400 to 329 × 10^3 (top to bottom) for the different arrays. The monolayer MoS_2 is overlaid in purple for clarity. In this way, we identify the optimal dosage and emitter yield. Moreover, the letters "TUM" are written with a constant dose of $\sigma = 0.3 \times 10^{13}$ cm^{-2} and are clearly visible as a bright emission from an ensemble of photon emitters. Importantly, our He-ion dose for the emitter generation is ~10^4–10^5 less compared to doses for which amorphization effects typically occur.[32]

By analyzing each irradiated position, we can statistically evaluate the overall percentage of activated fields for each set of

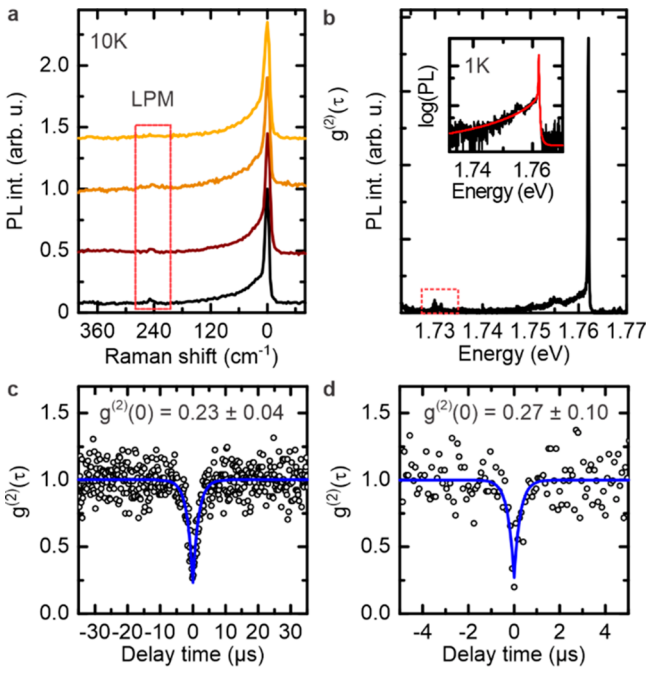

Figure 3. Photon antibunching of He-ion generated photon emitters in atomically thin MoS_2. (a) Photoluminescence spectra of four typical, spectrally clean emitters at 10 K with an fwhm of ~1.42 meV. The local phonon mode (LPM) at a Raman shift of ~248 cm^{-1} (energy detuning of ~31 meV) is highlighted. (b) Photoluminescence spectrum of an emitter at 1 K with an fwhm of 248 μeV and an LPM at around ~248 cm^{-1}. Inset: Same data on logarithmic scale fitted with an independent boson model. (c) Second-order correlation $g^{(2)}(\tau)$ function of an emitter from distribution I showing clear antibunching with $g^{(2)}(0)$ = 0.23 ± 0.04 and a lifetime of τ = 1.73 ± 0.15 μs at 5 K. (d) Second-order correlation with a value of $g^{(2)}(0)$ = 0.27 ± 0.10 and a lifetime of τ = 0.23 ± 0.05 μs of an emitter from distribution II.

https://dx.doi.org/10.1021/acsphotonics.0c01907
ACS Photonics 2021, 8, 669–677

Table 1. Summary of Different Approaches and Their Spatial Accuracy to Generate Selected Localized Photon Emitters in Diamond and 2D Materials[b]

	creation method	axial/lateral precision (nm/nm)	ZPL emission energy (eV)	inhomogeneous ensemble broadening (fwhm) (meV)	lifetime	countrate	Debye−Waller (DW) factor
NV	N beam[4]	(8[5]/10[33,34])	1.946[35]	NA	18 ns[36]	∼1·10^6 [36]	0.04[37] (77 K)
SiV	Si beam[38]	(70/32)[38]	∼1.653−1.698[39]	∼10[39]	0.2−2 ns[39]	∼5·10^6 [39]	0.75−0.88[39] (RT)
hBN	strain[14]	(75/100)[14]	∼1.99−2.34[14]	∼175[14]	2.5 ns[40]	∼4·10^7 [41]	0.82[18] (77 K)
	annealing/ e$^-$ beam[15,40]	random	∼1.59−2.25[42]	∼300[42]			
	growth[16]	random	∼2.101−2.175[16]	∼40[16]			
WSe_2	strain[12,13,20]	(150/60)[12]	∼1.51−1.68[12,13]	∼80[12,13]	0.3−10 ns[7,43]	∼3·10^6 [44]	0.6[44] (4.2 K)
WS_2	strain[12]	(150/60)[12]	∼1.82−2.03[12]	∼100[12]	NA	∼1·10^4 [12]	NA
$MoSe_2$	strain[45]	non-deterministic[45]	∼1.56−1.64[45]	∼40[45]	NA	∼7·10^3 [45]	NA
MoS_2	He-ion beam[23]	(0.7/10)[a28]	∼1.72−1.78[a]	∼31[a]	0.23−1.73 μs[a]	∼4·10^3 [23]	0.27[a] (1 K) 0.2[23] (10 K)
GaSe	strain[19,46]	non-deterministic[19]	∼1.7−2.0[19]	∼150[19]	1−22 ns[19,46]	∼10^3 [19]	NA

[a]This work. [b]For layered materials, we define the axial resolution of the emitters (0D state) by its planarity with respect to the host 2D material. For comparison, experimentally observed zero phonon line (ZPL) energies and inhomogeneous ensemble broadening are shown in addition to the typically observed Debye−Waller factor which represents the ratio of light emitted from the ZPL and the phonon side band. Note: While localized emission is observed in $MoSe_2$ and WS_2, photon antibunching is not reported as of yet.

doses and the number of photon emitters per spot (Figure 4b−g). A Poisson analysis (lines in Figure 4b−g) gives that 0.22 ± 0.06 emitters on average are generated at the lowest dose. The deviations from the Poisson distribution suggest that the generation events become statistically dependent especially for higher doses. For the latter, the spectral distinction of individual emitters starts to become challenging (cf. arrows in Figure 4i). However, for the lowest doses (<5.1k ions), single emitters can be straightforwardly identified (gray shaded area). The probability distribution for selected doses ranging from 400 to 329 × 10^3 ions per spot and the corresponding irradiated areas are highlighted in Figure 4a by dashed lines in the same colors. The total yield of activated fields (Figure 4h, black) increases monotonically from 20% to 60% throughout the range of doses used for He-ion irradiation. We find that, for the lowest dose of 400 ions per single irradiation (Figure 4b), about 18% of irradiated spots manifest in the generation of one emitter. For larger doses, this number increases to 37% for 82 × 10^3 ions (Figure 4h, cyan). Typical spectra for selected doses are shown in Figure 4i. All spectra show an emitter at a very similar detuning from the neutral exciton X.

The advantages of focused ion beam creation of photon emitters in an atomically thin material are summarized in Table 1 by comparing literature values of relevant parameters for the generation of color centers in diamond and layered materials. We obtain record high values for both axial and lateral positioning accuracy, while maintaining the planarity of the 2D material with very narrow inhomogeneous ensemble broadening and simultaneous high creation efficiencies of 18% for spectra with individual emission lines on single ion exposure spots. In all other 2D materials to date, localized emission is either non-deterministically observed across specific positions of exfoliated flakes, such as edges, wrinkles, or folds,[7,9−11,15,19,45−47] or induced through generation of strain potentials using prepatterned substrates, e.g., nanopillars with macroscopic feature sizes.[12−14,20] The strain field strongly varies in such devices, resulting in large variations of corresponding photon emission energies. Furthermore, for color centers in bulk diamond, due to the compound defect structure of vacancy and impurity atom, a post-annealing step is required to form color centers at the additional expense of positioning accuracy due to vacancy diffusion over macroscopic distances.[48] Moreover, ion straggling effects due to scattering events along the beam path further reduce both lateral and axial resolution,[37] which is negligibly small in a 2D material with the highly directed He-ion beam and the thin hBN cappings used. While recent reports comprise the improvement of lateral implantation precision with values down to 10 nm for NVs[33,34] and the creation of shallow defects 8 nm below the diamond surface by delta doping[5] and higher activation efficiencies for high energy ion beams,[49] for all results, an improvement of one parameter comes with the cost of either strongly diminished spatial accuracy, optical quality, or yield.

The ability to create localized photon emitters in already assembled van der Waals devices opens up a manifold of opportunities to investigate and control their optical properties in a context that is fully compatible with top down nanofabrication. Generally speaking, ideal single-photon sources need to emit photons on demand with a high purity and a near-unity indistinguishability besides of being scalable and interconnected with further quantum systems.[50,51] The demonstrated low adsorbate related background and the presented positioning of the He-ion induced photon emitters will allow for a detailed characterization in terms of indistinguishability and purity of their photon emission, e.g., by utilizing Hong−Ou−Mandel-type experiments.[51] With the presented generation yield of individual photon emitters, we envision a deterministic scaling of photon emitters by *in situ* monitoring in the HIM or by vacancy defect generation in a scanning tunneling microscope which further pushes the emitter generation to the atomistic limit. In particular, creation in as-fabricated field-switchable van der Waals devices for potential control of the defects charge state, integration in cavities, and waveguide with high Purcell enhancements for high photon emission rates and potential room-temperature operation or investigating superradiance effects of coherently coupled photon sources are straightforwardly achievable for the near future.

METHODS

Sample Fabrication. For the van der Waals heterostructures, we use MoS_2 bulk crystals from SPI supplies and high-quality hBN crystals from Takashi Taniguchi and Kenji

https://dx.doi.org/10.1021/acsphotonics.0c01907
ACS Photonics 2021, 8, 669−677

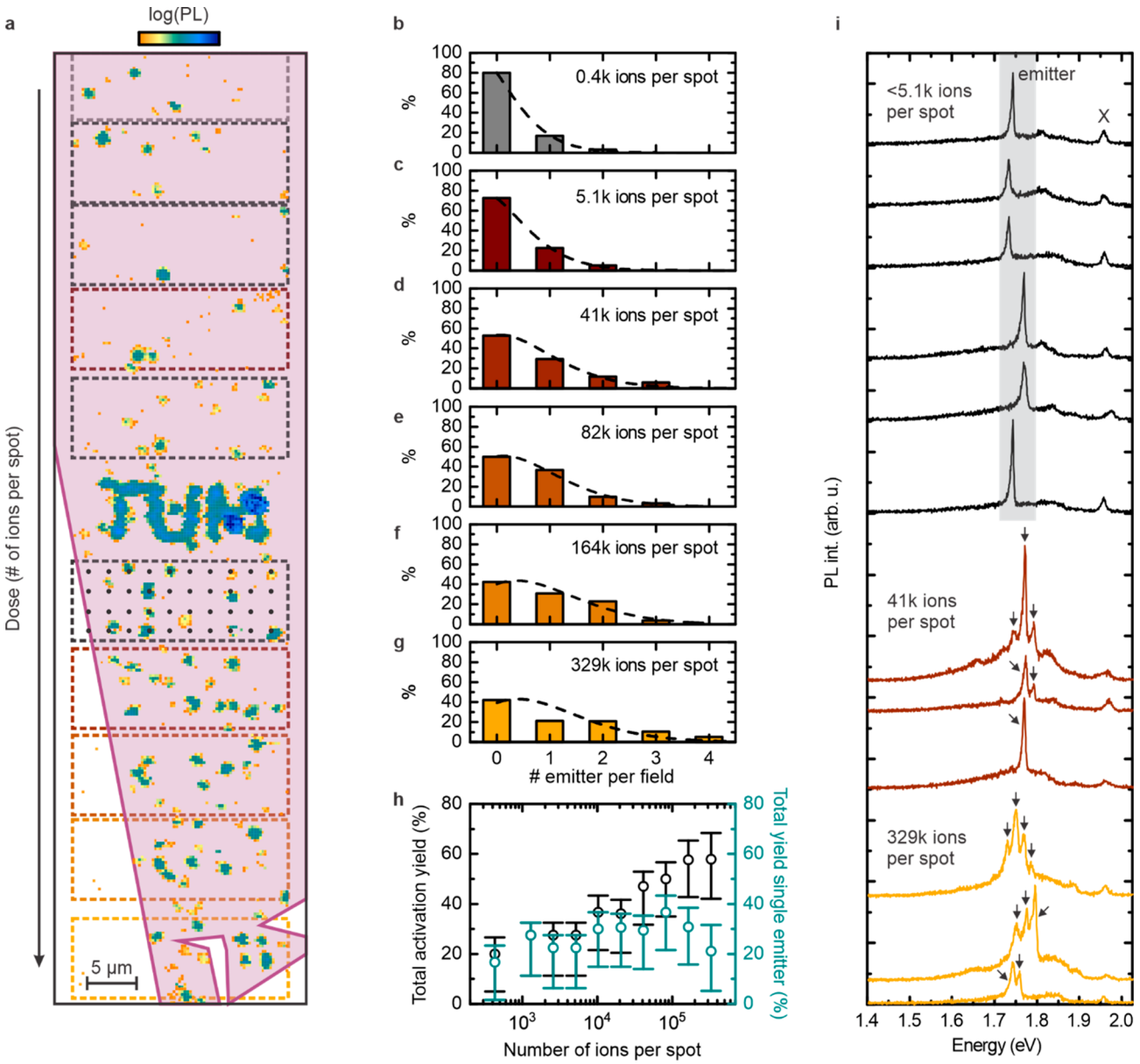

Figure 4. Positioned generation of He-ion induced photon emitters. (a) Spatially resolved and spectrally integrated low temperature (15 K) μ-PL mapping of a monolayer MoS_2 (purple area). The PL intensity is integrated in the spectral window of 1.7−1.88 eV. Defects are created through the hBN/MoS_2/hBN heterostructure with a tightly focused He-ion beam. The thickness of the top hBN layer is <15 nm. Arrays of He-ion spot exposures are arranged with a pitch of 2 μm (black dots) while the dose (number of ions per spot) increases from top to bottom. The "TUM" letters are written with a constant dose of $\sigma = 0.3 \times 10^{13}$ ions cm^{-2} to obtain ensemble defect emission. (b−g) Probability distribution of the number of photon emitters per irradiated spot for different dosages ranging from 400 to 329 × 10^3 ions per spot. For the lowest number of ions, about 18% of the activated spectra exhibit a single emission line, while spots exposed with 82 × 10^3 ions manifest in 37% probability to obtain individual photon emitters. Fields exposed to higher numbers of He ions are more likely to show multiple defect emission lines. Dashed lines are Poissonian fits giving the following number of emitters (per irradiated spot) per dose (b) 0.22 ± 0.06, (c) 0.32 ± 0.01, (d) 0.63 ± 0.05, (e) 0.69 ± 0.03, (f) 0.91 ± 0.10, and (g) 0.94 ± 0.19. (h) Total percentage of activated fields (black) and likelihood to obtain a single emitter (cyan). (i) Typical PL spectra reveal the neutral exciton X at 1.95 eV and the emitter emission around 1.75 eV. For low doses (<5.1 × 10^3 ions), spots show typically individual photon emitters at ∼1.75 (highlighted in gray) while fields with a higher dose (41 × 10^3 and 329 × 10^3 ions per spot) are more likely to show multiple emitters as highlighted by arrows.

Watanabe from the National Institute of Science in Tsukuba, Japan. To create heterostacks, we employ the dry viscoelastic stamping method to iteratively stack individual 2D materials on top of each other. Besides helium-ion irradiation, samples are not treated by other means.

Optical Spectroscopy. For the spatially resolved PL data, a continuous-wave 488 nm laser was used for excitation. The sample was cooled down to 10 K in a continuous flow cryostat (Janis ST-500). The laser was focused onto the sample with a microscope objective (NA = 0.42, 50×, Mitutoyo). Scanning was performed by a two axis scanning galvanometer mirror system (Thorlabs) combined with a 4f lens geometry. The emitted light was separated from the excitation path by a 50:50 beamsplitter and dispersed in a spectrometer (Spectra Pro HRS-300) and projected onto a charge coupled device CCD

https://dx.doi.org/10.1021/acsphotonics.0c01907
ACS Photonics 2021, 8, 669−677

(PIXIS). The excitation laser was blocked by a long-pass filter (RazorEdge LP 488).

The sample at 5 K (attoDry800) was excited using a HeNe laser. The emission was collected with a (50×, NA = 0.81, attocube) microscope objective, fiber-coupled, and filtered using two tunable band-pass filters. The fiber-based HBT setup consists of a 50:50 beamsplitter and two superconducting-nanowire single-photon detectors (Single Quantum) with efficiencies of 50%, 60%, timing jitters of 20 and 30 ps, and dark count rates of 0.006 and 0.017 cts/s.

μ-PL - spectroscopy at 1 K was performed in a cryogen-free dilution refrigerator operated at an elevated temperature of 1 K. Optical side access through anti-reflection coated windows was used to focus a continuous-wave 632 nm laser on the sample using a (50×, NA = 0.82, Partec) microscope objective.

Helium-Ion Microscopy. In order to generate the photon emitters, we used focused He-ion beam irradiation in a helium-ion microscope. For writing circular areas of different sizes, we used a beam current of I = 0.1 pA and a constant dose of 5 × 10^{12} ions/cm^2 and a beam spacing of 5 nm in x- and y-directions. For point shots, a beam current of I = 0.1 pA was used and the dwell time per spot was adjusted such that the desired number of ions was obtained at each spot. Unwanted irradiation was mitigated by using a large field-of-view for locating vdW heterostructures with background doses kept well below 10^{11} ions/cm^2. Emitters not matching with write patterns originate from the background dose and are accounted for with errors in Figure 4h.

■ ASSOCIATED CONTENT

Supporting Information

The Supporting Information is available free of charge at https://pubs.acs.org/doi/10.1021/acsphotonics.0c01907.

SRIM/TRIM simulation of He-ion beam trajectories, background estimation for PL spectra, control measurement to exclude defect emission from He-ion treated hBN, emission statistics of the emitters, and emitter spectra for antibunching (PDF)

■ AUTHOR INFORMATION

Corresponding Authors

Julian Klein − *Walter Schottky Institut und Physik Department, Technische Universität München, 85748 Garching, Germany; Munich Center of Quantum Science and Technology (MCQST), 80799 Munich, Germany; Department of Materials Science and Engineering, Massachusetts Institute of Technology, Cambridge, Massachusetts 02139, United States;* orcid.org/0000-0002-0873-8224; Email: jpklein@mit.edu

Alexander W. Holleitner − *Walter Schottky Institut und Physik Department, Technische Universität München, 85748 Garching, Germany; Munich Center of Quantum Science and Technology (MCQST), 80799 Munich, Germany;* orcid.org/0000-0002-8314-4397; Email: holleitner@wsi.tum.de

Authors

Lukas Sigl − *Walter Schottky Institut und Physik Department, Technische Universität München, 85748 Garching, Germany; Munich Center of Quantum Science and Technology (MCQST), 80799 Munich, Germany*

Samuel Gyger − *KTH Royal Institute of Technology, Department of Applied Physics, Albanova University Centre, 106 91 Stockholm, Sweden;* orcid.org/0000-0003-2080-9897

Katja Barthelmi − *Walter Schottky Institut und Physik Department, Technische Universität München, 85748 Garching, Germany; Munich Center of Quantum Science and Technology (MCQST), 80799 Munich, Germany*

Matthias Florian − *Institut für Theoretische Physik, Universität Bremen, 28334 Bremen, Germany*

Sergio Rey − *Walter Schottky Institut und Physik Department, Technische Universität München, 85748 Garching, Germany*

Takashi Taniguchi − *National Institute for Materials Science, Tsukuba, Ibaraki 305-0044, Japan;* orcid.org/0000-0002-1467-3105

Kenji Watanabe − *National Institute for Materials Science, Tsukuba, Ibaraki 305-0044, Japan;* orcid.org/0000-0003-3701-8119

Frank Jahnke − *Institut für Theoretische Physik, Universität Bremen, 28334 Bremen, Germany*

Christoph Kastl − *Walter Schottky Institut und Physik Department, Technische Universität München, 85748 Garching, Germany; Munich Center of Quantum Science and Technology (MCQST), 80799 Munich, Germany;* orcid.org/0000-0001-5309-618X

Val Zwiller − *KTH Royal Institute of Technology, Department of Applied Physics, Albanova University Centre, 106 91 Stockholm, Sweden*

Klaus D. Jöns − *KTH Royal Institute of Technology, Department of Applied Physics, Albanova University Centre, 106 91 Stockholm, Sweden;* orcid.org/0000-0002-5814-7510

Kai Müller − *Walter Schottky Institut und Physik Department, Technische Universität München, 85748 Garching, Germany; Munich Center of Quantum Science and Technology (MCQST), 80799 Munich, Germany*

Ursula Wurstbauer − *Institute of Physics, University of Münster, 48149 Münster, Germany*

Jonathan J. Finley − *Walter Schottky Institut und Physik Department, Technische Universität München, 85748 Garching, Germany; Munich Center of Quantum Science and Technology (MCQST), 80799 Munich, Germany*

Complete contact information is available at: https://pubs.acs.org/10.1021/acsphotonics.0c01907

Author Contributions

○J.K. and L.S. contributed equally and are both first authors. J.K., L.S., C.K., K.M., U.W., J.J.F., and A.W.H. conceived and designed the experiments; T.T. and K.W. provided hBN crystals; S.R. prepared the samples; J.K. performed He-ion irradiation; L.S., J.K., S.G., K.D.J., and K.B. performed the optical measurements; L.S., J.K., S.G., V.Z., and K.D.J. analyzed the data; M.F. and F.J. modeled spectral line shapes; J.K. wrote the manuscript with input from all authors. All authors reviewed the manuscript.

Notes

The authors declare no competing financial interest.

■ ACKNOWLEDGMENTS

The work was supported by Deutsche Forschungsgemeinschaft (DFG) through the German Excellence Strategy via the Munich Center for Quantum Science and Technology

(MCQST) - EXC-2111−390814868 and e-conversion − EXC 2089/1−390776260. We gratefully acknowledge support through TUM International Graduate School of Science and Engineering (IGSSE). We also gratefully acknowledge financial support from the European Union's Horizon 2020 research and innovation program under grant agreement No. 820423 (S2QUIP), the German Federal Ministry of Education and Research via the funding program Photonics Research Germany (contract number 13N14846), and the Bavarian Academy of Sciences and Humanities. J.K. acknowledges support from the Alexander von Humboldt Foundation. S.G. acknowledges funding from the Swedish Research Council under grant agreement 2016-06122 (Optical Quantum Sensing). K.D.J. acknowledges funding from the Swedish Research Council (VR) via the starting Grant HyQRep (ref 2018-04812) and The Göran Gustafsson Foundation (Swe-TeQ). M.F. and F.J. acknowledges support from the Deutsche Forschungsgemeinschaft (RTG 2247 "Quantum Mechanical Materials Modelling"). K.W. and T.T. acknowledge support from the Elemental Strategy Initiative conducted by the MEXT, Japan, and the CREST (JPMJCR15F3), JST.

REFERENCES

(1) Aharonovich, I.; Neu, E. Diamond Nanophotonics. *Adv. Opt. Mater.* **2014**, *2* (10), 911−928.
(2) Aharonovich, I.; Englund, D.; Toth, M. Solid-State Single-Photon Emitters. *Nat. Photonics* **2016**, *10* (10), 631−641.
(3) Atatüre, M.; Englund, D.; Vamivakas, N.; Lee, S.-Y.; Wrachtrup, J. Material Platforms for Spin-Based Photonic Quantum Technologies. *Nat. Rev. Mater.* **2018**, *3* (5), 38−51.
(4) Toyli, D. M.; Weis, C. D.; Fuchs, G. D.; Schenkel, T.; Awschalom, D. D. Chip-Scale Nanofabrication of Single Spins and Spin Arrays in Diamond. *Nano Lett.* **2010**, *10* (8), 3168−3172.
(5) Ohno, K.; Joseph Heremans, F.; Bassett, L. C.; Myers, B. A.; Toyli, D. M.; Bleszynski Jayich, A. C.; Palmstrøm, C. J.; Awschalom, D. D. Engineering Shallow Spins in Diamond with Nitrogen Delta-Doping. *Appl. Phys. Lett.* **2012**, *101* (8), 082413.
(6) Schröder, T.; Trusheim, M. E.; Walsh, M.; Li, L.; Zheng, J.; Schukraft, M.; Sipahigil, A.; Evans, R. E.; Sukachev, D. D.; Nguyen, C. T.; Pacheco, J. L.; Camacho, R. M.; Bielejec, E. S.; Lukin, M. D.; Englund, D. Scalable Focused Ion Beam Creation of Nearly Lifetime-Limited Single Quantum Emitters in Diamond Nanostructures. *Nat. Commun.* **2017**, *8* (1), 15376.
(7) Tonndorf, P.; Schmidt, R.; Schneider, R.; Kern, J.; Buscema, M.; Steele, G. A.; Castellanos-Gomez, A.; van der Zant, H. S. J.; Michaelis de Vasconcellos, S.; Bratschitsch, R. Single-Photon Emission from Localized Excitons in an Atomically Thin Semiconductor. *Optica* **2015**, *2* (4), 347.
(8) He, Y.-M.; Clark, G.; Schaibley, J. R.; He, Y.; Chen, M.-C.; Wei, Y.-J.; Ding, X.; Zhang, Q.; Yao, W.; Xu, X.; Lu, C.-Y.; Pan, J.-W. Single Quantum Emitters in Monolayer Semiconductors. *Nat. Nanotechnol.* **2015**, *10* (6), 497−502.
(9) Koperski, M.; Nogajewski, K.; Arora, A.; Cherkez, V.; Mallet, P.; Veuillen, J.-Y.; Marcus, J.; Kossacki, P.; Potemski, M. Single Photon Emitters in Exfoliated WSe_2 Structures. *Nat. Nanotechnol.* **2015**, *10* (6), 503−506.
(10) Chakraborty, C.; Kinnischtzke, L.; Goodfellow, K. M.; Beams, R.; Vamivakas, A. N. Voltage-Controlled Quantum Light from an Atomically Thin Semiconductor. *Nat. Nanotechnol.* **2015**, *10* (6), 507−511.
(11) Srivastava, A.; Sidler, M.; Allain, A. V.; Lembke, D. S.; Kis, A.; Imamoğlu, A. Optically Active Quantum Dots in Monolayer WSe_2. *Nat. Nanotechnol.* **2015**, *10* (6), 491−496.
(12) Palacios-Berraquero, C.; Kara, D. M.; Montblanch, A. R.-P.; Barbone, M.; Latawiec, P.; Yoon, D.; Ott, A. K.; Loncar, M.; Ferrari, A. C.; Atatüre, M. Large-Scale Quantum-Emitter Arrays in Atomically Thin Semiconductors. *Nat. Commun.* **2017**, *8* (1), 15093.
(13) Branny, A.; Kumar, S.; Proux, R.; Gerardot, B. D. Deterministic Strain-Induced Arrays of Quantum Emitters in a Two-Dimensional Semiconductor. *Nat. Commun.* **2017**, *8* (1), 15053.
(14) Proscia, N. V.; Shotan, Z.; Jayakumar, H.; Reddy, P.; Cohen, C.; Dollar, M.; Alkauskas, A.; Doherty, M.; Meriles, C. A.; Menon, V. M. Near-Deterministic Activation of Room-Temperature Quantum Emitters in Hexagonal Boron Nitride. *Optica* **2018**, *5* (9), 1128.
(15) Choi, S.; Tran, T. T.; Elbadawi, C.; Lobo, C.; Wang, X.; Juodkazis, S.; Seniutinas, G.; Toth, M.; Aharonovich, I. Engineering and Localization of Quantum Emitters in Large Hexagonal Boron Nitride Layers. *ACS Appl. Mater. Interfaces* **2016**, *8* (43), 29642−29648.
(16) Mendelson, N.; Xu, Z.-Q.; Tran, T. T.; Kianinia, M.; Scott, J.; Bradac, C.; Aharonovich, I.; Toth, M. Engineering and Tuning of Quantum Emitters in Few-Layer Hexagonal Boron Nitride. *ACS Nano* **2019**, *13* (3), 3132−3140.
(17) Gupta, S.; Yang, J.-H.; Yakobson, B. I. Two-Level Quantum Systems in Two-Dimensional Materials for Single Photon Emission. *Nano Lett.* **2019**, *19* (1), 408−414.
(18) Tran, T. T.; Bray, K.; Ford, M. J.; Toth, M.; Aharonovich, I. Quantum Emission from Hexagonal Boron Nitride Monolayers. *Nat. Nanotechnol.* **2016**, *11* (1), 37−41.
(19) Tonndorf, P.; Schwarz, S.; Kern, J.; Niehues, I.; Del Pozo-Zamudio, O.; Dmitriev, A. I.; Bakhtinov, A. P.; Borisenko, D. N.; Kolesnikov, N. N.; Tartakovskii, A. I.; Michaelis de Vasconcellos, S.; Bratschitsch, R. Single-Photon Emitters in GaSe. *2D Mater.* **2017**, *4* (2), 021010.
(20) Kern, J.; Niehues, I.; Tonndorf, P.; Schmidt, R.; Wigger, D.; Schneider, R.; Stiehm, T.; Michaelis de Vasconcellos, S.; Reiter, D. E.; Kuhn, T.; Bratschitsch, R. Nanoscale Positioning of Single-Photon Emitters in Atomically Thin WSe_2. *Adv. Mater.* **2016**, *28* (33), 7101−7105.
(21) Grosso, G.; Moon, H.; Lienhard, B.; Ali, S.; Efetov, D. K.; Furchi, M. M.; Jarillo-Herrero, P.; Ford, M. J.; Aharonovich, I.; Englund, D. Tunable and High-Purity Room Temperature Single-Photon Emission from Atomic Defects in Hexagonal Boron Nitride. *Nat. Commun.* **2017**, *8* (1), 705.
(22) Klein, J.; Kuc, A.; Nolinder, A.; Altzschner, M.; Wierzbowski, J.; Sigger, F.; Kreupl, F.; Finley, J. J.; Wurstbauer, U.; Holleitner, A. W.; Kaniber, M. Robust Valley Polarization of Helium Ion Modified Atomically Thin MoS_2. *2D Mater.* **2018**, *5* (1), 011007.
(23) Klein, J.; Lorke, M.; Florian, M.; Sigger, F.; Sigl, L.; Rey, S.; Wierzbowski, J.; Cerne, J.; Müller, K.; Mitterreiter, E.; Zimmermann, P.; Taniguchi, T.; Watanabe, K.; Wurstbauer, U.; Kaniber, M.; Knap, M.; Schmidt, R.; Finley, J. J.; Holleitner, A. W. Site-Selectively Generated Photon Emitters in Monolayer MoS_2 via Local Helium Ion Irradiation. *Nat. Commun.* **2019**, *10* (1), 2755.
(24) Klein, J.; Kerelsky, A.; Lorke, M.; Florian, M.; Sigger, F.; Kiemle, J.; Reuter, M. C.; Taniguchi, T.; Watanabe, K.; Finley, J. J.; Pasupathy, A. N.; Holleitner, A. W.; Ross, F. M.; Wurstbauer, U. Impact of Substrate Induced Band Tail States on the Electronic and Optical Properties of MoS_2. *Appl. Phys. Lett.* **2019**, *115* (26), 261603.
(25) Wierzbowski, J.; Klein, J.; Sigger, F.; Straubinger, C.; Kremser, M.; Taniguchi, T.; Watanabe, K.; Wurstbauer, U.; Holleitner, A. W.; Kaniber, M.; Müller, K.; Finley, J. J. Direct Exciton Emission from Atomically Thin Transition Metal Dichalcogenide Heterostructures near the Lifetime Limit. *Sci. Rep.* **2017**, *7* (1), 12383.
(26) Barja, S.; Refaely-Abramson, S.; Schuler, B.; Qiu, D. Y.; Pulkin, A.; Wickenburg, S.; Ryu, H.; Ugeda, M. M.; Kastl, C.; Chen, C.; Hwang, C.; Schwartzberg, A.; Aloni, S.; Mo, S.-K.; Frank Ogletree, D.; Crommie, M. F.; Yazyev, O. V.; Louie, S. G.; Neaton, J. B.; Weber-Bargioni, A. Identifying Substitutional Oxygen as a Prolific Point Defect in Monolayer Transition Metal Dichalcogenides. *Nat. Commun.* **2019**, *10* (1), 3382.
(27) Schuler, B.; Qiu, D. Y.; Refaely-Abramson, S.; Kastl, C.; Chen, C. T.; Barja, S.; Koch, R. J.; Ogletree, D. F.; Aloni, S.; Schwartzberg, A. M.; Neaton, J. B.; Louie, S. G.; Weber-Bargioni, A. Large Spin-Orbit Splitting of Deep In-Gap Defect States of Engineered Sulfur Vacancies in Monolayer WS 2. *Phys. Rev. Lett.* **2019**, *123* (7), 076801.

https://dx.doi.org/10.1021/acsphotonics.0c01907
ACS Photonics 2021, 8, 669−677

(28) Mitterreiter, E.; Schuler, B.; Cochrane, K. A.; Wurstbauer, U.; Weber-Bargioni, A.; Kastl, C.; Holleitner, A. W. Atomistic Positioning of Defects in Helium Ion Treated Single-Layer MoS_2. *Nano Lett.* **2020**, *20* (6), 4437−4444.
(29) Molina-Sánchez, A.; Wirtz, L. Phonons in Single-Layer and Few-Layer MoS 2 and WS 2. *Phys. Rev. B: Condens. Matter Mater. Phys.* **2011**, *84* (15), 155413.
(30) Wigger, D.; Schmidt, R.; Del Pozo-Zamudio, O.; Preuß, J. A.; Tonndorf, P.; Schneider, R.; Steeger, P.; Kern, J.; Khodaei, Y.; Sperling, J.; de Vasconcellos, S. M.; Bratschitsch, R.; Kuhn, T. Phonon-Assisted Emission and Absorption of Individual Color Centers in Hexagonal Boron Nitride. *2D Mater.* **2019**, *6* (3), 035006.
(31) Kretschmer, S.; Maslov, M.; Ghaderzadeh, S.; Ghorbani-Asl, M.; Hlawacek, G.; Krasheninnikov, A. V. Supported Two-Dimensional Materials under Ion Irradiation: The Substrate Governs Defect Production. *ACS Appl. Mater. Interfaces* **2018**, *10* (36), 30827−30836.
(32) Livengood, R.; Tan, S.; Greenzweig, Y.; Notte, J.; McVey, S. Subsurface Damage from Helium Ions as a Function of Dose, Beam Energy, and Dose Rate. *J. Vac. Sci. Technol. B Microelectron. Nanometer Struct.* **2009**, *27* (6), 3244.
(33) Bayn, I.; Chen, E. H.; Trusheim, M. E.; Li, L.; Schröder, T.; Gaathon, O.; Lu, M.; Stein, A.; Liu, M.; Kisslinger, K.; Clevenson, H.; Englund, D. Generation of Ensembles of Individually Resolvable Nitrogen Vacancies Using Nanometer-Scale Apertures in Ultrahigh-Aspect Ratio Planar Implantation Masks. *Nano Lett.* **2015**, *15* (3), 1751−1758.
(34) Scarabelli, D.; Trusheim, M.; Gaathon, O.; Englund, D.; Wind, S. J. Nanoscale Engineering of Closely-Spaced Electronic Spins in Diamond. *Nano Lett.* **2016**, *16* (8), 4982−4990.
(35) Gruber, A. Scanning Confocal Optical Microscopy and Magnetic Resonance on Single Defect Centers. *Science* **1997**, *276* (5321), 2012−2014.
(36) Schröder, T.; Gädeke, F.; Banholzer, M. J.; Benson, O. Ultrabright and Efficient Single-Photon Generation Based on Nitrogen-Vacancy Centres in Nanodiamonds on a Solid Immersion Lens. *New J. Phys.* **2011**, *13* (5), 055017.
(37) Pezzagna, S.; Rogalla, D.; Wildanger, D.; Meijer, J.; Zaitsev, A. Creation and Nature of Optical Centres in Diamond for Single-Photon Emission—Overview and Critical Remarks. *New J. Phys.* **2011**, *13* (3), 035024.
(38) Schröder, T.; Trusheim, M. E.; Walsh, M.; Li, L.; Zheng, J.; Schukraft, M.; Sipahigil, A.; Evans, R. E.; Sukachev, D. D.; Nguyen, C. T.; Pacheco, J. L.; Camacho, R. M.; Bielejec, E. S.; Lukin, M. D.; Englund, D. Scalable Focused Ion Beam Creation of Nearly Lifetime-Limited Single Quantum Emitters in Diamond Nanostructures. *Nat. Commun.* **2017**, *8*, 15376.
(39) Neu, E.; Steinmetz, D.; Riedrich-Möller, J.; Gsell, S.; Fischer, M.; Schreck, M.; Becher, C. Single Photon Emission from Silicon-Vacancy Colour Centres in Chemical Vapour Deposition Nano-Diamonds on Iridium. *New J. Phys.* **2011**, *13* (2), 025012.
(40) Tran, T. T.; Elbadawi, C.; Totonjian, D.; Lobo, C. J.; Grosso, G.; Moon, H.; Englund, D. R.; Ford, M. J.; Aharonovich, I.; Toth, M. Robust Multicolor Single Photon Emission from Point Defects in Hexagonal Boron Nitride. *ACS Nano* **2016**, *10* (8), 7331−7338.
(41) Li, X.; Scully, R. A.; Shayan, K.; Luo, Y.; Strauf, S. Near-Unity Light Collection Efficiency from Quantum Emitters in Boron Nitride by Coupling to Metallo-Dielectric Antennas. *ACS Nano* **2019**, *13* (6), 6992−6997.
(42) Xu, Z.-Q.; Elbadawi, C.; Tran, T. T.; Kianinia, M.; Li, X.; Liu, D.; Hoffman, T. B.; Nguyen, M.; Kim, S.; Edgar, J. H.; Wu, X.; Song, L.; Ali, S.; Ford, M.; Toth, M.; Aharonovich, I. Single Photon Emission from Plasma Treated 2D Hexagonal Boron Nitride. *Nanoscale* **2018**, *10* (17), 7957−7965.
(43) Luo, Y.; Shepard, G. D.; Ardelean, J. V.; Rhodes, D. A.; Kim, B.; Barmak, K.; Hone, J. C.; Strauf, S. Deterministic Coupling of Site-Controlled Quantum Emitters in Monolayer WSe_2 to Plasmonic Nanocavities. *Nat. Nanotechnol.* **2018**, *13* (12), 1137−1142.
(44) Kumar, S.; Brotóns-Gisbert, M.; Al-Khuzheyri, R.; Branny, A.; Ballesteros-Garcia, G.; Sánchez-Royo, J. F.; Gerardot, B. D. Resonant Laser Spectroscopy of Localized Excitons in Monolayer WSe_2. *Optica* **2016**, *3* (8), 882.
(45) Branny, A.; Wang, G.; Kumar, S.; Robert, C.; Lassagne, B.; Marie, X.; Gerardot, B. D.; Urbaszek, B. Discrete Quantum Dot like Emitters in Monolayer MoSe 2: Spatial Mapping, Magneto-Optics, and Charge Tuning. *Appl. Phys. Lett.* **2016**, *108* (14), 142101.
(46) Tonndorf, P.; Del Pozo-Zamudio, O.; Gruhler, N.; Kern, J.; Schmidt, R.; Dmitriev, A. I.; Bakhtinov, A. P.; Tartakovskii, A. I.; Pernice, W.; Michaelis de Vasconcellos, S.; Bratschitsch, R. On-Chip Waveguide Coupling of a Layered Semiconductor Single-Photon Source. *Nano Lett.* **2017**, *17* (9), 5446−5451.
(47) He, Y.-M.; Clark, G.; Schaibley, J. R.; He, Y.; Chen, M.-C.; Wei, Y.-J.; Ding, X.; Zhang, Q.; Yao, W.; Xu, X.; Lu, C.-Y.; Pan, J.-W. Single Quantum Emitters in Monolayer Semiconductors. *Nat. Nanotechnol.* **2015**, *10* (6), 497−502.
(48) Santori, C.; Barclay, P. E.; Fu, K.-M. C.; Beausoleil, R. G. Vertical Distribution of Nitrogen-Vacancy Centers in Diamond Formed by Ion Implantation and Annealing. *Phys. Rev. B: Condens. Matter Mater. Phys.* **2009**, *79* (12), 125313.
(49) Pezzagna, S.; Naydenov, B.; Jelezko, F.; Wrachtrup, J.; Meijer, J. Creation Efficiency of Nitrogen-Vacancy Centres in Diamond. *New J. Phys.* **2010**, *12* (6), 065017.
(50) Santori, C.; Fattal, D.; Vučković, J.; Solomon, G. S.; Yamamoto, Y. Indistinguishable Photons from a Single-Photon Device. *Nature* **2002**, *419* (6907), 594−597.
(51) Schöll, E.; Hanschke, L.; Schweickert, L.; Zeuner, K. D.; Reindl, M.; Covre da Silva, S. F.; Lettner, T.; Trotta, R.; Finley, J. J.; Müller, K.; Rastelli, A.; Zwiller, V.; Jöns, K. D. Resonance Fluorescence of GaAs Quantum Dots with Near-Unity Photon Indistinguishability. *Nano Lett.* **2019**, *19* (4), 2404−2410.

https://dx.doi.org/10.1021/acsphotonics.0c01907
ACS Photonics 2021, 8, 669−677